– Supporting Information –
Threading of unconcatenated ring polymers at high concentrations: double-folded *vs.* time-equilibrated structures

Jan Smrek*
Max Planck Institut for Polymer Research, Ackermannweg 10, D-55128 Mainz, Germany and Faculty of Physics, University of Vienna, Boltzmanngasse 5, A-1090 Vienna, Austria

Kurt Kremer†
Max Planck Institut for Polymer Research, Ackermannweg 10, D-55128 Mainz, Germany

Angelo Rosa‡
SISSA (Scuola Internazionale Superiore di Studi Avanzati), Via Bonomea 265, 34136 Trieste, Italy

CONTENTS

I. MODELS AND METHODS

A. Melt conformations of ring polymers from the interacting branched polymer (IBP) model

1. Construction of the model

Equilibrated conformations of branched polymers in melt were prepared according to the algorithm by Rosa and Everaers [1]. The algorithm consists of four steps:

Step 1: Melt of lattice trees – We construct randomly-branching polymers on the $3d$-cubic lattice by resorting to a modified version of the Monte Carlo (MC) "amoeba" algorithm by Seitz and Klein [2] with periodic boundary conditions. The length of the unit cell of the lattice is equal to the Kuhn length, $\ell_K/\sigma = 10$, of the final ring polymer model. Here, σ is the unit of length (=monomer diameter) in the *final* ring polymer model. The average Kuhn segments density per unit cell is $\rho_K \ell_K^3 = 5$.

Initially, polymers are randomly placed on the lattice as standard random-walks. At each MC step, one of the monomers with functionality = 1 is randomly selected and attached to any randomly chosen monomer of the same chain with functionality < 3. The move is accepted with probability

$$\mathrm{acc}(i \to f) = \min\left\{1, \frac{n_1(i)}{n_1(f)} \exp\left[-\mu_{\mathrm{br}}\left(n_3(f) - n_3(i)\right)\right] \exp\left[-v_K \sum_{site \in lattice} \left(n_K(f, site)^2 - n_K(i, site)^2\right)\right]\right\} \quad (1)$$

where:

(1) $n_1(i)$ and $n_3(i)$ (respectively, $n_1(f)$ and $n_3(f)$) are the total numbers of 1- and 3-functional monomers in the initial (respectively, final) state.

(2) $n_K(i, site)$ (respectively, $n_K(i, site)$) is the total number of Kuhn segments inside the unit cell centered at the corresponding lattice site in the initial (resp., final) state.

(3) $\mu_{\mathrm{br}} = -2.0$ and $v_K = 4k_BT$ are two phenomenological parameters. The first is chosen by imposing that the fraction of branching points in each tree is $\approx 40\%$. The second fixes the scale for the free energy penalty accounting for excluded volume between overlapping pairs

* jan.smrek@univie.ac.at
† kremer@mpip-mainz.mpg.de
‡ anrosa@sissa.it

of Kuhn segments within the same unit cell.

Step 2: Conversion of lattice trees into off-lattice bead-spring branched polymers – To resolve the spatial overlap between polymer conformations, we replace each Kuhn segment in the original lattice model with 5 linearly connected beads of diameter $= 2\sigma$. This is to assure that in the step 3 below we can build non-overlapping ribbons inside the corresponding occupied volume. Overlaps are then removed by the gentle "push-off" Molecular Dynamics (MD) procedure described in [3, 4] and implemented in LAMMPS [5]. The procedure ensures that chain monomers are displaced by spatial distances of the order of their own linear size.

The Kremer-Grest-like [3] model adopted for the off-lattice branched conformations accounts for the connectivity, bending rigidity, excluded volume and local topology conservation of polymers:

1. Bonded interactions between pairs of monomers at spatial separation r are modeled by the finitely extensible nonlinear elastic (FENE) potential. It is made of two terms. The first, attractive, is given by:

$$U_{\rm FENE}(r) = \begin{cases} -0.5kR_0^2 \ln\left(1-((r-\Delta)/R_0)^2\right) & r \le R_0 \\ \infty & r > R_0 \end{cases} , \tag{2}$$

where $k = 30\epsilon/\sigma^2$ is the spring constant, $\epsilon = 1k_BT$ fixes the energy scale and the maximum extension of the bond $\Delta + R_0$ is determined by choosing $\Delta/\sigma = 1$ and $R_0/\sigma = 1.5$. The second, repulsive, is described by the Lennard-Jones (LJ) expression:

$$U_{\rm LJ}(r) = \begin{cases} 4\epsilon\left[\left(\frac{\sigma}{r-\Delta}\right)^{12} - \left(\frac{\sigma}{r-\Delta}\right)^{6} + \frac{1}{4}\right] & r \le r_c \\ 0 & r > r_c \end{cases} , \tag{3}$$

where $r_c/\sigma = 2^{1/6}$.

2. Bending rigidity between consecutive triplets of neighbouring beads along the ring with spatial coordinates $(\vec{r}_{i-1}, \vec{r}_i, \vec{r}_{i+1})$ are modeled according to:

$$U_{\rm bend}(\theta) = k_\theta\, \theta^2 \,, \tag{4}$$

where $\theta_i = \cos^{-1}\frac{(\vec{r}_{i+1}-\vec{r}_i)\cdot(\vec{r}_i-\vec{r}_{i-1})}{|\vec{r}_{i+1}-\vec{r}_i|\,|\vec{r}_i-\vec{r}_{i-1}|}$ is the angle formed by the adjacent bonds along the chain and $k_\theta = 30\, k_BT$ is the bending prefactor. The large value adopted for the stiffness is based on the need for preventing excessive polymer crumpling during simulations [1].

3. The push-off procedure consists of two stages. During the first stage, non-bonded excluded volume interactions are described by the non-diverging, soft-core potential:

$$U_{\rm soft}(r) = A\left(1+\cos(\pi r/r_c^{\rm soft})\right) \,, \tag{5}$$

with $r_c^{\rm soft}/\sigma = 2.4225$ and A ramped from 0 to $100k_BT$ in an MD run of a few $\tau_{\rm MD} \equiv \sigma\sqrt{m/\epsilon}$ where m is the "conventional" monomer mass. During this run, overlapping monomers are pushed away from each other. This run is followed by a second one of same duration and with non-bonded interactions changed to the full LJ potential, Eq. (3).

Step 3: Generation of double-folded ring conformations – Non-overlapping branched polymers can now be transformed into bead-spring, crumpled ring conformations. To do so, we start from a (randomly-chosen) 1-functional monomer of each branched polymer and we keep placing monomers by moving along the branched backbone while remaining at a distance of $\sigma/2$ from it. During the process the distance between nearest neighbors monomers is bound to the range $[0.8\sigma - 1.2\sigma]$ so to avoid unnaturally stretched chain bonds. At branching points (3-functional sites), we choose randomly amongst the two possible remaining directions. This construction ends when the proximities of the initial monomer are finally reached. We end the protocol by checking once again if nearest neighbor distances along the chain stay in the interval $[0.8\sigma - 1.2\sigma]$. If not, we correct for this wherever needed. At the end of this step, the total number of monomers of each system is four times those of corresponding systems of branched backbones. Finally, Kuhn segments density is $\rho_K \ell_K^3 = 10$ [1, 6].

Step 4: Density relaxation on the entanglement scale – Bonded and non-bonded interactions between monomers in ring polymers are described by the same Eqs. (2) and (3) with $\Delta = 0$. Bending stiffness is instead replaced by the expression:

$$U_{\rm bend}(\theta) = k_\theta\,(1-\cos\theta) \,, \tag{6}$$

corresponding to the fiber Kuhn length, ℓ_K, given by [4]:

$$\frac{\ell_K}{\sigma} = \frac{1+\langle\cos\theta\rangle}{1-\langle\cos\theta\rangle} \tag{7}$$
$$\langle\cos\theta\rangle = \frac{1+e^{2\beta k_\theta}(\beta k_\theta - 1)+\beta k_\theta}{(e^{2\beta k_\theta}-1)\beta k_\theta} \,.$$

For the present model $k_\theta = 5k_BT$ and Eq. (7) implies that the fiber Kuhn length $\ell_K/\sigma = 10$.

To achieve complete system relaxation, we perform a short ($= 10\tau_{\rm MD}$) MD run under the condition that monomers cannot move more than 0.05σ at each integration time step. Finally, density fluctuations up to the entanglement scale are levelled-off by performing standard MD runs up to 0.75 of the (estimated) entanglement time $\tau_e \approx 1600\tau_{\rm MD}$ [6].

In this work, we have considered the same ring polymer solutions studied in Ref. [1]. A summary of the rings and systems sizes considered as well as further details concerning their numerical analysis are summarized in the IBP-model column of Table S1.

2. Molecular Dynamics simulations details

The static and kinetic properties of the polymers are studied using fixed-volume and constant-temperature

MD simulations (NVT ensemble) with implicit solvent and periodic boundary conditions.

MD simulations are performed using the LAMMPS engine [5]. The equations of motion are integrated using a velocity Verlet algorithm, in which all beads are weakly coupled to a Langevin heat bath with a local damping constant $\Gamma = 0.5/\tau_{\rm MD}$. The integration time step is set to $\Delta\tau = 0.006\,\tau_{\rm MD}$ for push-off procedures and $\Delta\tau = 0.012\,\tau_{\rm MD}$ for relaxation runs.

B. Concentrated solutions and melts of ring polymers equilibrated by Molecular Dynamics computer simulations

In this work, we have considered two distinct sets – named hereafter "EQ MD 1" and "EQ MD 2", respectively – of solutions of ring polymers equilibrated by large-scale Molecular Dynamics (MD) computer simulations. The two sets are described by two different microscopic polymer models, each model characterized by a specific local chain stiffness (or Kuhn length of the chain, ℓ_K) and overall monomer density (ρ).

To ensure a proper comparison between the two data sets, the measured observables have been discussed in terms of the polymer mass (L_c) measured in entanglement lengths, $Z \equiv \frac{L_c}{L_e}$, where L_e is the entanglement length [8]. For polymer contour lengths larger than L_e, the microscopic details of the employed polymer model become irrelevant and the predicted properties of the solution universal.

In general, the entanglement length, L_e, is a complicated function of the parameters of the solution like chain stiffness and monomer density. For loosely entangled solutions as the ones considered in this work, L_e can be calculated from a "primitive path" analysis [9] according to the interpolation formula:

$$\frac{L_e}{\ell_K} = \left(\frac{1}{0.06(\rho_K \ell_K^3)}\right)^{2/5} + \left(\frac{1}{0.06(\rho_K \ell_K^3)}\right)^{2}, \qquad (8)$$

where $\rho_K = \rho/(\ell_K/\sigma)$ is the density of Kuhn segments.

In the following, we provide more details on the two polymer models considered in this work. A concise summary of the systems analyzed and the statistics of the different polymer configurations is given in Table S1.

EQ MD 1 – The first data set (see Refs. [7, 10]) is for semi-flexible ring polymers described by the classical Kremer-Grest polymer model [3] with dense melt conditions (monomer density $\rho = 0.85\sigma^{-3}$) and bending stiffness defined by Eq. (6) with $k_\theta = 1.5 k_B T$ corresponding (Eq. (7)) to the Kuhn length $\ell_K \approx 2.56\sigma$. Accordingly (Eq. (8)), $L_e \approx 28\sigma$.

Data for $Z = 14, 29, 57$ were produced by long, standard MD computer simulations as described in [10]. Instead, since relaxation times for the largest rings with $Z = 114$ ($L_c = 3200\sigma$) would be computationally prohibitive, we have adopted the alternative strategy of doubling the contour length of each ring conformation with $Z = 57$ ($L_c = 1600\sigma$). However, bare isotropic inflation of the system by a factor of 2 followed by insertion of a bead in between each two consecutive beads would just create threading statistics biased by the smaller system. To avoid this, we adopted the following procedure: On each ring a segment of length $ds = 25\sigma$ was selected at random, a bead was inserted in between each two beads of the segment and the ring re-bonded to incorporate the new beads. The insertion was performed by inflating the bead diameter of the newly introduced beads from 0.5σ to σ in 50 steps of duration $5\tau_{MD}$ each. After the insertion, the system was relaxed for $(20ds^2)\tau_{MD}$ which is long enough (i) to completely relax the structures on scales of ds, because this is below the entanglement length and (ii) to reproduce the conformational statistics as found empirically when doubling shorter systems. The insertion and relaxation was repeated 64 times to reach the new length of $N = 3200$. Let us stress that in each round the doubling segment was chosen uniformly randomly on the ring. This ensures that we are not biased by the threading present in the original system of rings. The doubling process was ran at constant pressure maintained by Berendsen barostat with τ_P equal to the square root of twice the number of particles. Here the parameter τ_P governs the relaxation of the box size by rescaling all coordinates by a factor of $\mu = 1 - \frac{\beta dt}{3\tau_P}(P_0 - P)$ as $\vec{r}_{\rm new} = \mu\,\vec{r}_{\rm old}$, where $dt = 0.005\tau_{MD}$ is the time step used, β is the isothermal compressibility (set to unity) and $P_0 - P$ is the difference between the target and the actual pressure (see [11] for details). After the ring mass of $N = 3200$ monomers was reached, the system was switched from NPT to NVT simulation by re-scaling all coordinates by a common factor in order to match target monomer density $= 0.85\sigma^{-3}$. The factor was typically less than 1.001 as the pressure of the system was almost perfectly equilibrated. The system was then run for another $2 \times 10^6 \tau_{MD}$. The total run time was about $2.8 \times 10^6 \tau_{MD}$, which is significantly shorter than the predicted diffusive relaxation time but it is about the same as the predicted conformational relaxation time for these polymer rings [10].

EQ MD 2 – The second data set is for MD simulations of rings whose initial states correspond to double-folded polymers on branched primitive trees (IBP-model, Sec. SI A). In this case, $\ell_K = 10\sigma$ and $\rho = 0.1\sigma^3$ imply (see Eq. (8)) $L_e = 4\ell_K = 40\sigma$. The total run time for each of these simulations was fixed being equal to $1.2 \times 10^7 \tau_{\rm MD}$ or $\approx 7500\tau_e$.

As anticipated in the main text, ring dynamics is discussed in terms of two observables [10]:

(1) Rings thermal diffusion can be used to monitor systems equilibration. Accordingly, we define the time mean-square displacement [3]:

$$\langle g_3(t)\rangle \equiv \frac{1}{M}\sum_{m=1}^{M}\frac{1}{T-t}\int_0^{T-t}(\vec{r}^{\,m}_{cm}(t+t') - \vec{r}^{\,m}_{cm}(t'))^2 dt' \qquad (9)$$

where t is the lag-time, T is the length of the MD trajec-

EQ MD 1 Halverson *et al.* [7]					EQ MD 2 Rosa and Everaers [1]					IBP-model Rosa and Everaers [1]				
N	Z	M	#pairs	#frames	N	Z	M	#pairs	#frames	N	Z	M	#pairs	#frames
400	14	200	16800	10	205	5	500	1200	1	63	1.5	160	7800	100
800	29	200	26800	10	613	15	256	1700	1	103	2.5	64	5600	100
1600	57	200	39500	10	1531	38	256	3200	1	205	5	32	5200	100
3200*	114	200	49300	10	4692†	115	256	5700	1	613	15	256	10000	10
										1531	38	256	19200	10
										4692	115	256	39200	10
										9179	225	256	15500	3
										18357	450	128	9200	3
										36711	900	64	4700	3

Table S 1. Summary of rings solutions considered in this work, see also Secs. I A and I B and the original works [1, 7] for more details. (a) N and (b) $Z \equiv L_c/L_e = (N\sigma)/L_e$: ring masses, expressed in number of monomers and in number of entanglement lengths, respectively. (c) M: total number of rings constituting the solution for the corresponding ring mass. (d) #pairs: total number of ring pairs showing mutual penetrations. (e) #frames: total number of independent frames or snapshots analyzed (for EQ MD 2 there is one frame analyzed at each studied time point). *EQ MD 1 data with $Z = 114$ were obtained by doubling the lengths of the rings with $Z = 57$ by resorting to the procedure described in Sec. SI B: we stress that results for these systems have to be taken with care since the numerical procedure does not guarantee the reach of complete equilibration. †EQ MD 2 data with $Z = 115$ are for MD simulations spanning only a very few single ring diffusion times (Fig. S1): consequently, these polymers are not perfectly equilibrated either and corresponding results need to be also taken with care.

Z	α_Q	α_{n_p}	$\tau^{\rm th}_{{\rm rel},Q}\,[\tau_e]$	$\tau^{\rm th}_{{\rm rel},n_p}\,[\tau_e]$	$\tau^{\rm diff}_{\rm rel}\,[\tau_e]$	$\tau^{\rm int}_{\rm rel}\,[\tau_e]$
5	0.30	0.05	$\lesssim 8\times10^0$	$\lesssim 8\times10^0$	$\approx 4\times10^0$	$\approx 1\times10^0$
15	0.35 ± 0.05	0.06 ± 0.01	$\approx 8\times10^1$	$\approx 6\times10^1$	$\approx 5\times10^1$	$\approx 1\times10^1$
38	0.32 ± 0.01	0.06 ± 0.01	$\approx 6\times10^2$	$\approx 3\times10^2$	$\approx 5\times10^2$	$\approx 7\times10^1$
115†	0.250 ± 0.003	–	$\approx 1\times10^4$	–	$\approx 7\times10^3$	$\approx 4\times10^2$

Table S 2. Summary of threading dynamics and dynamical properties of rings of total contour length Z. The reported results were obtained from analyzing MD simulations from data set EQ MD 2. (a) α_Q: Dynamic exponent describing early time relaxation of $\bar{Q}(t) \sim (t/\tau_e)^{\alpha_Q}$, Eq. (2) of the main text. (b) α_{n_p}: Dynamic exponent describing early time relaxation of $\bar{n}_p(t) \sim (t/\tau_e)^{\alpha_{n_p}}$, Eq. (3) of the main text. (c) $\tau^{\rm th}_{{\rm rel},Q}$: Threading relaxation time from time behavior of $\bar{Q}(t)$. (d) $\tau^{\rm th}_{{\rm rel},n_p}$: Threading relaxation time from time behavior of $\bar{n}_p(t)$. (e) $\tau^{\rm diff}_{\rm rel}$: Diffusion relaxation time. Its scaling behavior with Z is compatible with the one reported for the EQ MD 1 data set (see Fig. 5 in [10]). (f) $\tau^{\rm int}_{\rm rel}$: Internal relaxation time. †EQ MD 2 data with $Z = 115$ are for MD simulations spanning only a very few single ring diffusion times (Fig. S1): consequently, these polymers are not perfectly equilibrated and corresponding α_Q, α_{n_p} and relaxation time-scales must be taken with care.

tory and $\vec{r}^{\,m}_{cm}(t) \equiv \frac{1}{N}\sum_{i=1}^{N} \vec{r}^{\,m}_i(t)$ is the spatial position of the center of mass of the m-th ring of the system whose i-th monomer has spatial coordinates $\vec{r}^{\,m}_i(t)$. $\langle g_3(t)\rangle$ is then compared to the time evolution of the ring mean-square gyration radius:

$$\langle R^2_g(t)\rangle \equiv \frac{1}{MN}\sum_{m=1}^{M}\sum_{i=1}^{N}(\vec{r}^{\,m}_i(t) - \vec{r}^{\,m}_{cm}(t))^2\,. \qquad (10)$$

The ring relaxation time $\tau^{\rm diff}_{\rm rel}$ is then defined by the relationship:

$$\langle g_3(\tau^{\rm diff}_{\rm rel})\rangle \equiv \langle R^2_g(\tau^{\rm diff}_{\rm rel})\rangle\,. \qquad (11)$$

As shown in Fig. S1, our trajectories are long enough to achieve good equilibration for rings with $Z = 5, 15, 38$. Conversely, rings with $Z = 115$ are approximately equilibrated and corresponding data need to be taken with care. Specific data for $\tau^{\rm diff}_{\rm rel} = \tau^{\rm diff}_{\rm rel}(Z)$ are summarized in Table S2.

(2) The second observable was introduced in Ref. [10] as a mean to characterize rings internal motion. For any ring in solution at time t we consider an arbitrarily chosen pair of vectors $\vec{d}_1 = \vec{d}_1(t)$ and $\vec{d}_2 = \vec{d}_2(t)$, each vector connecting two monomers of the same ring separated by a contour length $Z/2$. The two vectors are chosen so that the tails are separated by a contour length $= Z/4$. By taking the cross product $\vec{c}(t) = \vec{d}_1(t) \times \vec{d}_2(t)$, the internal relaxation time $\tau^{\rm int}_{rmrel}$ is defined by the integral over time of the corresponding correlation function:

$$\tau^{\rm int}_{\rm rel} \equiv \int_0^\infty \frac{\langle \vec{c}(t)\cdot\vec{c}(0)\rangle}{\langle c(0)^2\rangle}dt\,. \qquad (12)$$

Numerical evaluations of Eq. (12) at each Z have been performed over the corresponding full MD trajectory, by stopping the integration whenever the relative error on the correlation function becomes $> 20\%$. This choice appears reasonable as $\frac{\langle \vec{c}(t)\cdot\vec{c}(0)\rangle}{\langle c(0)^2\rangle} = \mathcal{O}(10^{-2})$ at the cut-off

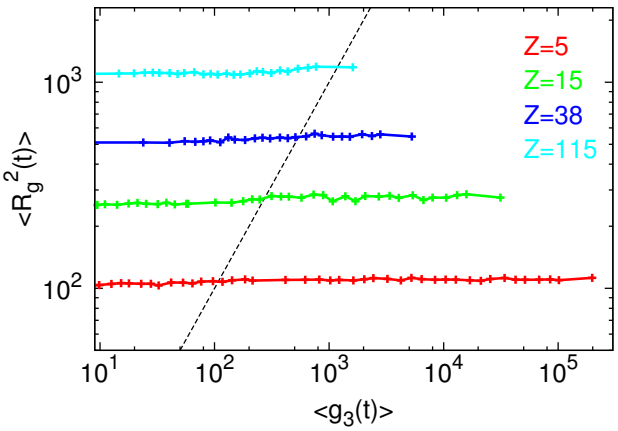

Fig. S 1. Comparing time evolutions of the mean-square gyration radius, $\langle R_g^2(t)\rangle$, *vs.* mean-square displacement of the ring center of mass, $\langle g_3(t)\rangle$. The dashed line corresponds to the curve $y = x$, and its crossings with the MD points imply that rings have moved, on average, over distances larger than their own typical sizes.

for all Z's. Our final results are summarized in Table S2: in agreement with Ref. [10], $\tau_{\rm rel}^{\rm int}(Z) < \tau_{\rm rel}^{\rm diff}(Z)$.

C. Construction of minimal surfaces for ring polymers

To obtain the minimal surfaces spanned on MD-equilibrated and branched ring polymers in non-prohibitive computing time, we follow a slightly modified version of the numerical procedure described in [12].

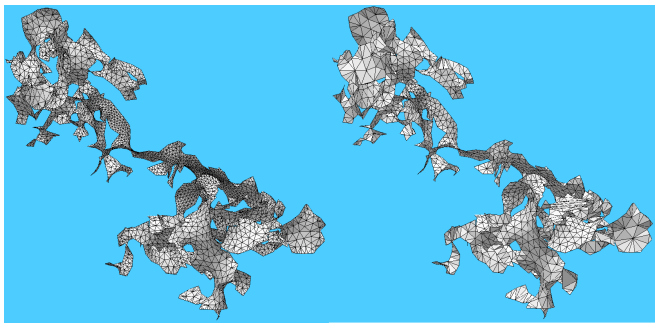

Fig. S 2. Comparison of the minimal surface from the original minimization algorithm presented in Ref. [12] (left) and the one obtained from the coarser procedure adopted in this work (right) for a single ring with $L_c = 800\sigma$ ($Z = 29$) extracted from data set EQ MD 1 (Sec. SI B).

Firstly, we initialize the surface as a union of L_c triangles, where each triangle is spanned on two successive monomer positions and the center of the mass of the ring. Next, we refine the surface once, by subdividing each triangle into four smaller ones. The surfaces, represented by $4L_c$ triangles, are subsequently minimized by mean curvature flow with restructuring of the mesh towards Delaunay triangulation (equiangulation), weeding out of small triangles and vertex averaging, as discussed in [12]. After the initial minimization (that takes about 20000 steps of the mean curvature flow) the relative surface area change is being measured during the run. Surface evolution is stopped when the relative surface area does not change by more than 0.1% over 240 steps with equiangulations and, in case of decreasing time step, together with vertex averaging. We have found empirically that the above procedure produces surfaces close enough to a (local) minimum that is characterized by a vast majority of vertices ($> 99\%$) with the absolute value of the mean curvature smaller than 0.01. As shown in[12] the use of several different protocols for simulated annealing ensures that the procedure leads sufficiently close to the minimal surface. The minimal surfaces presented here are slightly coarser than the ones presented in [12], mainly because of using only one mesh refinement instead of two. Yet, the past and the present methodologies give remarkably close results, as illustrated in Fig. S2. The distribution of the minimal areas is similar in both cases and the mean is higher by only about 4% for coarser surfaces. As a final check, we have also verified that the threading statistics is not sensitive to these small changes (Fig. S3).

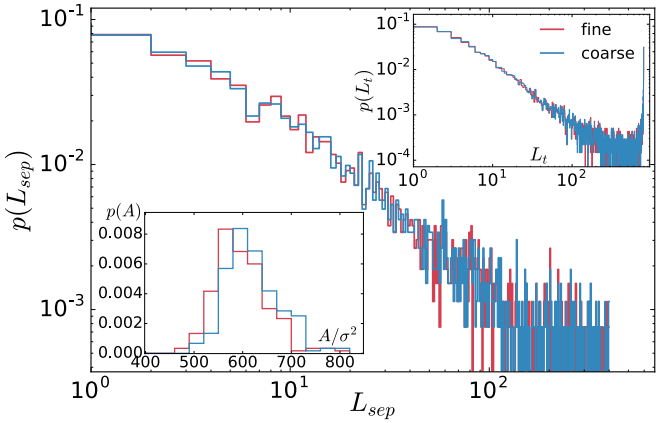

Fig. S 3. Comparison of the statistics for ring minimal surfaces as calculated according to: the original ("fine", red lines) algorithm proposed in Ref. [12] and the novel ("coarse", blue lines) procedure adopted in this work (Sec. SI C). Results are for MD-equilibrated rings with $L_c = 800\sigma$ ($Z = 29$) extracted from data set EQ MD 1 (Sec. SI B). Main plot: Probability distribution functions, $p(L_{\rm sep})$, for the separation length. Top inset: Probability distribution functions, $p(L_t)$, for the threading length. Bottom inset: Probability distribution functions, $p(A)$, for the minimal surface.

The following script (in Surface Evolver language) has been used to minimize the surfaces.

```
dumpfile:= sprintf "%s%s",datafilename,".dmp"
zeroar:=0;
old_area:=total_area;
arr:=1;
r; u 10;
{
  {V 10; u 10;} 10;
    K 0.2;
```

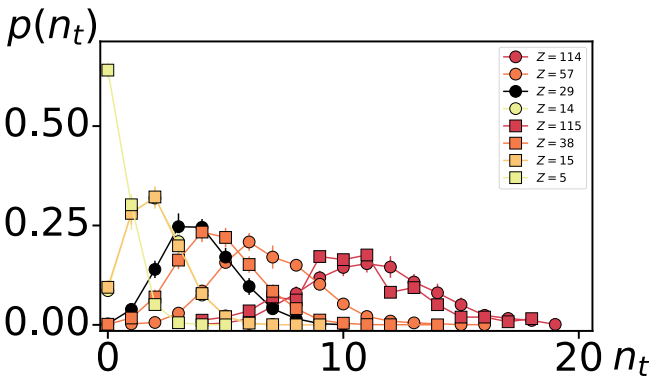

Fig. S 4. Normalized histograms of the number of neighbors, n_t, threaded by a ring for the two MD-equilibrated sets.

```
} 2;
{
  {
    {
      {u 5; g 10;} 2;
        if scale<0.1 then V ;
    } 5;
        foreach facet ff do
        {
          if ff.area==0 then print ff.id; w 0.01; break
        }
  } 10;
  dissolve edges;
  dissolve vertices;
  K 0.2;
} 3;
{
  {V 10; u 10; g 20;} 10;
  foreach facet ff do
    {
      if ff.area==0 then print ff.id; w 0.01; break
    }
} 10;
cycle_number:=0;
while arr>0.0001 do
  {
    old_area:= total_area;
    {
      { u 10; g 30; if scale<0.1 then V ; } 8;
      ta:=total_area;
      arr:=(old_area-ta)/ta;
      cycle_number:=cycle_number+1;
      if cycle_number>20 then
        {
          print datafilename >> outfile;
          break;
        }
    };
  };
u 5;
dissolve edges;
dissolve vertices;
u 5;
foreach facet ff do
  {
    if ff.area==0 then {g 100; w 0.001; break;}
  };
foreach facet ff do
  {
    if ff.area==0 then {zeroar:=1; break;}
  };
if zeroar==0 then
{
  {V; u;} 5;
  dissolve edges;
  dissolve vertices;
  dump dumpfile;
};
  print cycle_number;
q 3;
```

For few surfaces, this procedure was unable to converge due to internal surface evolver error (when trying to free a loop edge). In those few cases the w commands were set to 0.1, 0.001 or 0.0001 which solved the issue.

D. Threading detection

We define the penetration of the minimal surface of ring A by ring B *iff* a line segment between any two consecutive monomers of ring B intersect the internal area of any triangle from the triangulation of the minimal surface of ring A. As we label the line segments of B, it is straightforward to compute the (threading) length between two successive penetrations. We observe that a ring can also penetrate its own surface, however, in this work, we focus only on inter-ring threadings and we do not take self-threadings into account.

Determining the relative position of a line segment and a triangle is a standard problem in computer graphics that can be addressed in various ways (see e.g. one pedagogical approach in the appendix of work [13]).

In this work, we follow the algorithm presented in [14] that uses Plücker coordinates and the side operator:

- Plücker coordinates are a six-dimensional representation of a line segment a defined by two boundary points in $3d$ space $\vec{p} = (p_x, p_y, p_z)$ and $\vec{q} = (q_x, q_y, q_z)$. Each Plücker coordinate is one determinant of the 2×2 minor of the matrix

$$\begin{bmatrix} p_x & p_y & p_z & 1 \\ q_x & q_y & q_z & 1 \end{bmatrix}. \tag{13}$$

  Explicitly the coordinates of the line segment a are $a = (p_x q_y - q_x p_y, p_x q_z - q_x p_z, p_x - q_x, p_y q_z - q_y p_z, p_z - q_z, q_y - p_y)$. Sometimes another representation with clearer geometrical meaning is used $a = (\vec{p} - \vec{q}, \vec{p} \times (\vec{p} - \vec{q}))$, which differs only by permutation and signs.

- The side operator between two lines a and b is a permuted inner product in the six-dimensional space defined as $s(a, b) = a_0 b_1 + a_1 b_2 + a_2 b_3 + a_3 b_4 + a_4 b_5 + a_5 b_0$.

It can be shown that if all side operators of the line segment with the three triangle edges have the same sign, the line intersects the inner area of the triangle. From the values of the side operators one can extract more information of the relative positions of the line and the triangle such as the intersection at a vertex of the triangle (see [14] for details).

E. More details on threading statistics

From the presented statistics, it is not clear what fraction of its neighbors each ring threads. To quantify it, we have constructed histograms of the number of threaded neighbors $p(n_t)$ of a ring (Fig. S4) for the two sets of MD-equilibrated systems. As for the average number of times a ring penetrates the minimal surface of any other single ring ($\bar{n}_p$, Fig. 2 in the main text), we considered a neighbor to be threaded, only if at least one threading

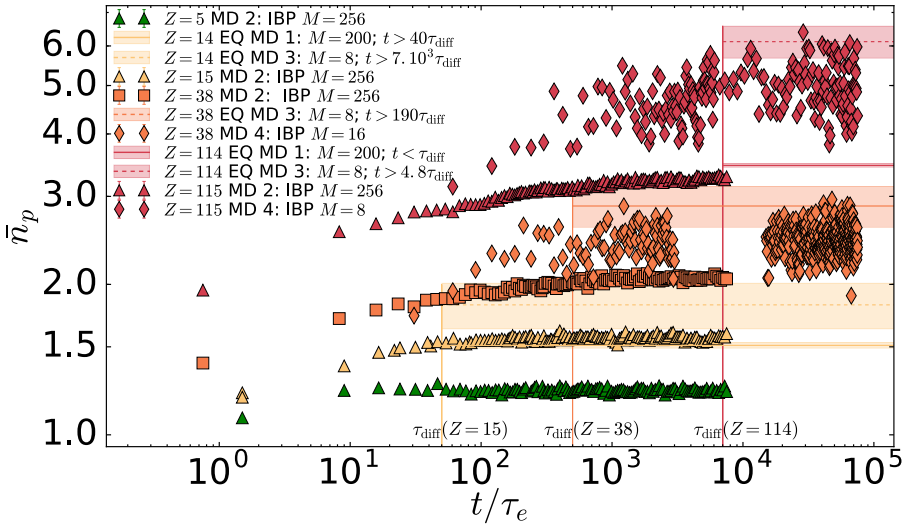

Fig. S 5. Time evolution of the mean number of penetrations, $\bar{n}_p(t)$, for various polymer models and setups. The color-shaded regions with horizontal lines represent the range (line is the mean, shading is the standard deviation) of equilibrium values of $\bar{n}_p$ as extracted from EQ MD 1 (solid line) and EQ MD 3 (dashed line) (see Sec. SII for more information on the additional data sets used). The time value in the label of the equilibrium data indicates, the time steps of the configurations used to obtain the mean equilibrium value. Each equilibrium region starts only at the diffusion relaxation time of the given Z. The diamond symbols represent data set EQ MD 4 and the other symbols are for data set EQ MD 2.

length L_t that contributes to L_{sep} (Eq. (1) in the main text) is *longer* than the entanglement length L_e. Notice that if threadings of any length were considered, as it was done in [12], the mean values of n_t agree with the data reported there (see Fig. 2a of that paper). In this case though, $p(n_t)$ for the EQ MD 1 data set would not agree with the EQ MD 2 data set because of natural differences in the microscopic details of the two models. With the new definition adopted here, we see that the two data sets agree very well (Fig. S4, see for instance the overlap between the two results for $Z = 114$ (EQ MD 1) and $Z = 115$ (EQ MD 2)).

In general, the n_t distributions appear unimodal for all Z. Only the very short rings ($Z \leq 15$) have non-vanishing value at $n_t = 0$. This means that every ring threads at least one neighbor, but often many neighbors. Surprisingly, the longest rings ($Z = 114$) have still higher average $\bar{n}_t$ than for $Z = 57$, although in the asymptotic limit $Z \to \infty$, one would expect this number to saturate due to the compact regime of the ring size ($R_g \sim N^\nu$ with $\nu = 1/3$). Interestingly, the variance of the n_t distribution grows with Z, which could have an important effect on the dynamics. We do not evaluate the fraction of neighbors that are threaded as this should depend on how we define a neighbor. In [7] the neighbor number $K(Z)$ is defined as the rings with center of mass within distance R_g. There the $K(57) \simeq 16$. Here, we see that when neglecting the short threadings, every ring threads fewer rings than K. On the other hand when threadings of any length are considered, the n_t is larger than K (not shown), because also short threadings for distances larger than R_g contribute.

II. ROLE OF NUMBER OF CHAINS IN $\bar{n}_p$ STATISTICS

We investigated briefly what is the effect of small number of chains on the threading statistics. We used the polymer model of EQ MD 2 and run MD to equilibrate two more sets of systems: (*i*) EQ MD 3: the starting configurations are (Hilbert or Moore) space-filling curves (SFC) as detailed in [1] with $M = 8$ chains each and for $Z = 14$, 38 and 115 and (*ii*) EQ MD 4: the starting configurations are IBP as in EQ MD 2, but the number of chains is $M = 16$ for $Z = 38$ and $M = 8$ for $Z = 115$. Fig. S5 summarizes our findings:

1. The equilibrium values of EQ MD 1 is below the equilibrium value of EQ MD 3 for both, the $Z = 15$, and for $Z = 115$. We speculate that this is because in this case the low chain number $M = 8$ causes that each chain interacts with itself through periodic boundary conditions and this could cause a "more open" conformation which is thus more easily threaded by other chains.

2. The $\bar{n}_p$ of late ($t > 10^4\tau_e$) EQ MD 4 simulation for $Z = 38$ with $M = 16$ is below the EQ MD 3 with $M = 8$ and above EQ MD 2 with $M = 256$, which supports the hypothesis above.

3. The equilibrium values of $\bar{n}_p$ for systems with $M = 200$ and $M = 256$ chains agree.

4. The $\bar{n}_p$ of late ($t > 10^4\tau_e$) EQ MD 4 simulation for $Z = 115$ with $M = 8$ tends toward the EQ MD 3 for this Z as expected, but probably more than one diffusion times are needed to fully equilibrate the system.

[1] A. Rosa and R. Everaers, "Ring polymers in the melt state: the physics of crumpling," Phys. Rev. Lett. **112**, 118302 (2014).

[2] W. A. Seitz and D. J. Klein, "Excluded volume effects for branched polymers," J. Chem. Phys. **75**, 5190–5193 (1981).

[3] K. Kremer and G. S. Grest, "Dynamics of entangled linear polymer melts: A molecular-dynamics simulation," J. Chem. Phys. **92**, 5057–5086 (1990).

[4] R. Auhl, R. Everaers, G. S. Grest, K. Kremer, and S. J. Plimpton, "Equilibration of long chain polymer melts in computer simulations," J. Chem. Phys. **119**, 12718–12728 (2003).

[5] S. Plimpton, "Fast parallel algorithms for short range molecular dynamics," J. Comp. Phys. **117**, 1–19 (1995).

[6] A. Rosa and R. Everaers, "Structure and dynamics of interphase chromosomes," Plos Comput. Biol. **4**, e1000153 (2008).

[7] J. D. Halverson, W. B. Lee, G. S. Grest, A. Yu. Grosberg, and K. Kremer, "Molecular dynamics simulation study of nonconcatenated ring polymers in a melt. I. Statics," J. Chem. Phys. **134**, 204904 (2011).

[8] R. Everaers, S. K. Sukumaran, G. S. Grest, C. Svaneborg, A. Sivasubramanian, and K. Kremer, "Rheology and microscopic topology of entangled polymeric liquids," Science **303**, 823–826 (2004).

[9] N. Uchida, G. S. Grest, and R. Everaers, "Viscoelasticity and primitive-path analysis of entangled polymer liquids: from f-actin to polyethilene," J. Chem. Phys. **128**, 044902 (2008).

[10] J. D. Halverson, W. B. Lee, G. S. Grest, A. Yu. Grosberg, and K. Kremer, "Molecular dynamics simulation study of nonconcatenated ring polymers in a melt. II. Dynamics," J. Chem. Phys. **134**, 204905 (2011).

[11] H. J. C. Berendsen, J. P. M. Postma, W. F. van Gunsteren, A. DiNola, and J. R. Haak, "Molecular dynamics with coupling to an external bath," J. Chem. Phys. **81**, 3684–3690 (1984).

[12] J. Smrek and A. Yu. Grosberg, "Minimal surfaces on unconcatenated polymer rings in melt," ACS Macro Lett. **5**, 750–754 (2016).

[13] A. Narros, A. J. Moreno, and C. N. Likos, "Effects of knots on ring polymers in solvents of varying quality," Macromolecules **46**, 3654–3668 (2013).

[14] S. Lazard, `https://members.loria.fr/SLazard/ARC-Visi3D/Pant-project/files/Line_Triangle.html`, 18/8/2001 (accessed 11/2018).